ACS OMEGA

http://pubs.acs.org/journal/acsodf

Article

Identification of Phosphorylation and Other Post-Translational Modifications in the Central C4C5 Domains of Murine Cardiac Myosin Binding Protein C

Chang Yoon Doh, Katherine L. Dominic, Caitlin E. Swanberg, Nikhil Bharambe, Belinda B. Willard, Ling Li, Rajesh Ramachandran, and Julian E. Stelzer*

Cite This: *ACS Omega* 2022, 7, 14189−14202

Read Online

ACCESS | Metrics & More | Article Recommendations | Supporting Information

ABSTRACT: Cardiac myosin binding protein C (cMyBPC) is a critical multidomain protein that modulates myosin cross bridge behavior and cardiac contractility. cMyBPC is principally regulated by phosphorylation of the residues within the M-domain of its N-terminus. However, not much is known about the phosphorylation or other post-translational modification (PTM) landscape of the central C4C5 domains. In this study, the presence of phosphorylation outside the M-domain was confirmed in vivo using mouse models expressing cMyBPC with nonphosphorylatable serine (S) to alanine substitutions. Purified recombinant mouse C4C5 domain constructs were incubated with 13 different kinases, and samples from the 6 strongest kinases were chosen for mass spectrometry analysis. A total of 26 unique phosphorylated peptides were found, representing 13 different phosphorylation sites including 10 novel sites. Parallel reaction monitoring and subsequent mutagenesis experiments revealed that the S690 site (UniProtKB O70468) was the predominant target of PKA and PKG1. We also report 6 acetylation and 7 ubiquitination sites not previously described in the literature. These PTMs demonstrate the possibility of additional layers of regulation and potential importance of the central domains of cMyBPC in cardiac health and disease. Data are available via ProteomeXchange with identifier PXD031262.

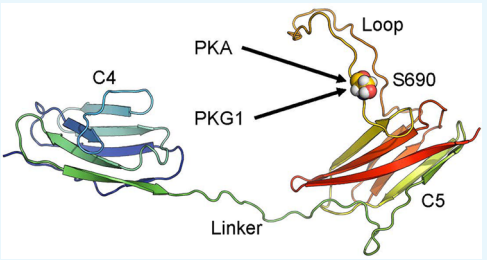

INTRODUCTION

Cardiac myosin binding protein C (cMyBPC) is a critical regulatory protein in cardiac muscle.[1,2] It consists of 8 immunoglobulin domains and 3 fibronectin type III domains, connected by linker residues.[2] It regulates cardiac contractility in response to inotropic stimuli through phosphorylation and other post-translational modifications (PTMs).[2−8] The phosphorylation of the M-domain of cMyBPC via cAMP-dependent protein kinase (PKA) has been the most extensively studied PTM and has shown importance in normal cardiac function[9] by relieving the constraints on myosin S2 and accelerating cross bridge cycling.[4,9−16] In particular, phosphorylation at serine (S) residues S273, S282, and S302 (mouse residue numbering, e.g. UniProtKB O70468, unless indicated otherwise) has been implicated in many important regulatory functions in the heart.[4,12,15,17,18] Recent reports also indicate that PKA-mediated S307 phosphorylation in vitro may contribute to the normal physiological function and regulation of murine cMyBPC.[19] More broadly, cMyBPC has been shown to be differentially phosphorylated in animal models of myocardial stunning and models of age-related cardiac dysfunction.[20,21] Furthermore, cardiac hypertrophy and heart failure have been associated with reduced overall cMyBPC phosphorylation levels,[22−26] and decreased cMyBPC phosphorylation is correlated with dysfunction in ischemia.[27,28]

Given the strong evidence that implicates phosphorylation as a modulator of the structure and function of cMyBPC in physiological and pathological cardiac conditions, significant effort has been devoted to elucidating the precise mechanisms of the phosphorylation sites in the M-domain. In contrast, relatively little is known about the phosphorylation or other PTM landscape, structure, or function of the central domains of cMyBPC.[3,29] Two unique features are present in the C4 and C5 domains: an elongated linker region between C4 and C5 and a cardiac isoform specific loop region in the middle of the C5 domain.[30] The C5 domain's cardiac-specific loop is highly dynamic and extended, and it seems to lack any defined secondary structures.[31] Although the exact function of the loop remains to be elucidated, it has been speculated that it may function as a stable scaffold for cardiac-specific ligand interactions of signal transduction molecules, perhaps as a site of kinase docking and phosphorylation.[3] Additionally, a recent study showed that cMyBPC forms bent conformations,

Received: February 8, 2022
Accepted: April 5, 2022
Published: April 18, 2022

60% with one hinge (forming a V-shape) and 40% with two hinges.[29] Based on measured lengths of the hinge arms, the two hinge domains are likely C1C2 and C4C5,[29] where the M-domain and the linker between C4 and C5 are located. Thus, it seems that the linker may provide a high degree of flexibility.[32] We hypothesized that these structural alterations may be regulated through phosphorylation and other PTMs.

To this end, we aimed to characterize precise phosphorylation sites of the murine cMyBPC C4C5 domains using mass spectrometry analysis, along with identification of kinase specificity. We also aimed to identify the site-specific phosphorylation contributions through mutagenesis and kinase experiments. Our results showed 13 total phosphorylation sites found in the C4C5 domains, and 10 novel sites not previously described in the literature. We also show that functionally important kinases such as PKA and PKG target only a few residues which contribute the most to the overall phosphorylation of the C4C5 domains, suggesting that these residues may be important in regulating cMyBPC structure and function. We also report other novel PTMs, including 6 acetylation and 7 ubiquitination sites in the C4C5 domains.

RESULTS AND DISCUSSION

Quantification of Basal Myofilament Phosphorylation Levels. The transgenic phospho-ablated 3SA mouse models showed a 57% basal phosphorylation level compared to WT mice (normalized phospho-stain/Coomassie signals of 1.00 ± 0.16 for WT vs 0.57 ± 0.11 for 3SA, $p < 0.05$). Additionally, the 4SA injected KO hearts showed a 56% basal phosphorylation level compared with the FL injected KO hearts (normalized phospho-stain/Coomassie signals of 1.00 ± 0.16 for KO^{FL} vs 0.56 ± 0.13 for 4SA, $p < 0.05$). The sequences used in generating the AAV9 vectors are shown in Figure S1. Representative gels images are shown in Figure 1.

The function of cMyBPC is known to be affected by N-terminal phosphorylation, specifically within the M-domain.[19,33,34] It is notable that only 3−4 main sites (S273, S282, S302, and S307) contribute to ∼44% of all basal cMyBPC phosphorylation, consistent with previous reports.[4,6] However, these experiments support the idea that there may be additional physiologically important phosphorylation sites in the rest of the protein, accounting for ∼56% of basal phosphorylation. For example, a study involving recombinant C1C2 domains with 4SD mutations showed complete ablation of phosphorylation signal even with PKA treatment.[19] This evidence indicates that there are no more PKA-targets in the C1C2 domains, and any additional PKA-induced phosphorylation sites are outside of the C1C2 domains.

In Vitro Kinase Experiments Showed Kinase-Specific Phosphorylation of Murine C4C5 Domains of cMyBPC. The recombinant mouse C4C5 protein was generated (Figure S2), purified, and determined to be 90−95% pure by Coomassie stain. C4C5 was confirmed to be well-structured via far-UV circular dichroism (Figure S3, Table S1). The C4C5 constructs were then treated with 13 different kinases each with its own control and stained with phospho-stain in order to explore the landscape of phosphorylation in the central region (Figure 2A,B). The kinases and concentrations used in the screening experiments are reported in Table S2 and Table S3. The phospho-stain showed some signal in the control samples, indicating a baseline level of phosphorylation. The strongest six kinases showed the following fold-increase in the total relative phosphorylation levels: RSK2 (2.8 fold increase), PKA (2.5), and PKG1 (2.2), AMPK (2.0), and PKD2 (1.6), and CK2 (1.4) (Figure 2C).

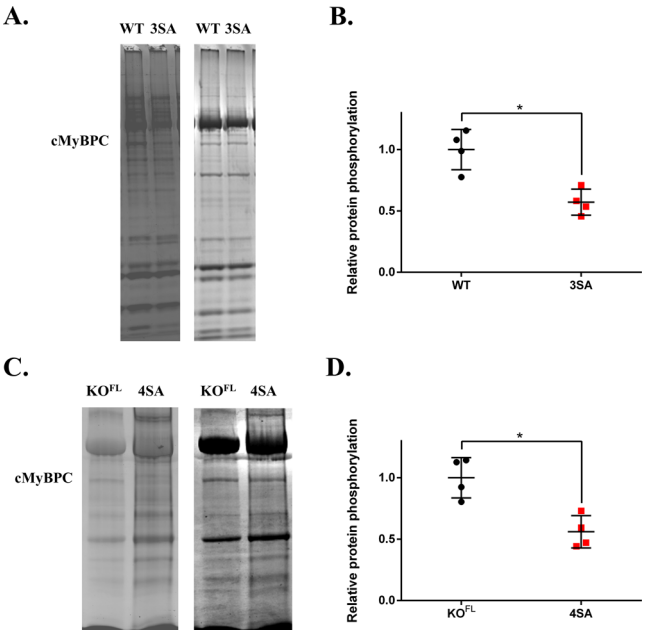

Figure 1. cMyBPC phosphorylation status of WT/3SA mouse models and KO^{FL}/4SA-injected hearts. (A) Representative phospho-stained (left) and Coomassie stained (right) cardiac myofibrils from WT and 3SA mouse lines. (B) Quantification of the relative protein phosphorylation of WT and 3SA ($n = 4$). The intensity of the Pro-Q-band was normalized to the Coomassie band intensity. (C) Representative phospho-stained (left) and Coomassie stained (right) cardiac myofibrils from KO hearts that were injected with FL (KO^{FL}) and 4SA AAV9 vectors. (D) Quantification of the relative protein phosphorylation of KO^{FL} and 4SA ($n = 4$). The intensity of the Pro-Q-band was normalized to the Coomassie band intensity. Values are expressed as mean ± SD. Significance was determined by a two-tailed t test. * $p < 0.05$ versus either WT or KO^{FL} group.

Interestingly, the six kinases mentioned above have been found to play important roles in the N-terminal domains. PKA has been found to phosphorylate S273, S282, S302, and S307 in addition to many other sites,[3,25,35] whereas other kinases such as RSK2, PKD2, CK2, PKG1 have been found to be have more complex roles in phosphorylating certain sites in the M-domain.[36] RSK2 phosphorylation of S282 is associated with reduction in calcium sensitivity and enhanced cross bridge kinetics.[37] PKD has been found to phosphorylate S302 selectively[38−40] and to play a role in stress response, cardiac hypertrophy, and angiogenesis.[36,37] CK2 has been shown to phosphorylate the S282 site in addition to other sites in the C0C2 domains, although its functional importance has yet to be determined.[25] It has been reported to be involved in proper embryonic heart development[41] and modulation of cardiac growth factor signaling.[42] Recently, PKG1a has been shown to phosphorylate all three M-domain sites (S273, S282, S302) in vitro, and also to increase S273 phosphorylation in response to left ventricular pressure overload.[43] Although AMPK has not been found to phosphorylate cMyBPC specifically, it has been implicated in the induction of hypertrophy and increase in metabolic demand seen in hypertrophic cardiomyopathy.[44] C4C5 samples treated with the above six kinases were used for further mass spectrometry analysis because of their physiological relevance.

https://doi.org/10.1021/acsomega.2c00799
ACS Omega 2022, 7, 14189−14202

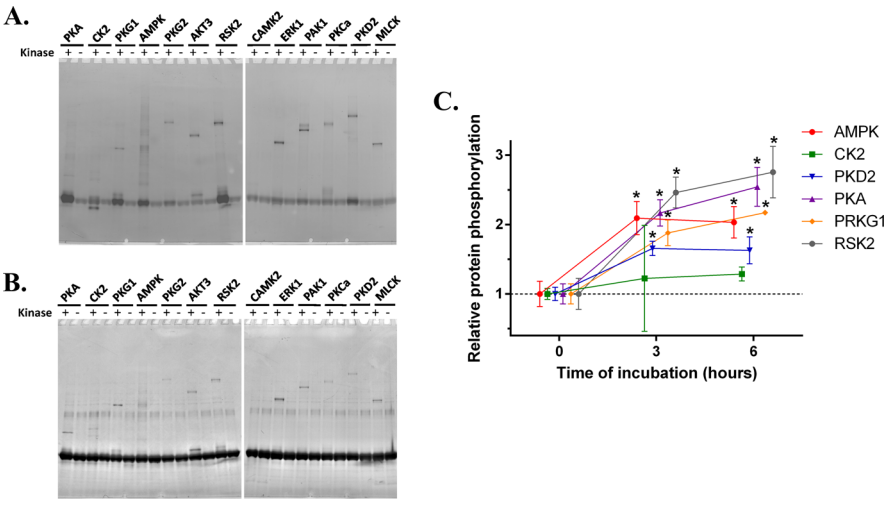

Figure 2. Representative phospho-stain (A) and Coomassie stained (B) gels of the C4C5 domains of murine cMyBPC incubated in the presence (+) and absence (−) of the corresponding kinase. Phospho-Tag Phosphoprotein Gel Stain from ABP Biosciences was used for these experiments. (C) Averaged relative protein phosphorylation of C4C5 protein over a 3 and 6 h time course. Data were normalized to the initial incubation at 0 h. Because the experiments were done separately for 3 and 6 h, statistical comparisons between 0 vs 3 h and 0 vs 6 h were made using a two-tailed *t* test. * indicates statistical significance ($p < 0.05$). Data presented as mean ± SEM ($n = 3–4$).

Table 1. Unique Phosphopeptides Identified in the C4C5 Domains of Murine cMyBPC[a]

site	phosphopeptide sequence	peptide start−end	[M + H]	*m*/*z*	*z*	Δ*m*, ppm	retention time (min)
S546	(MoHHHHHH)KLEVYQpSIADLAVGAK	(Mo-His_6- tags) 540−555	2754.30826	689.33294	4	0.61	86.3532
	LEVYQpSIADLAVGAK	541−555	1656.82443	828.91739	2	1.85	82.4590
	LEVYQpSIADLAVGAKDQAVFK	541−561	2345.17885	782.39719	3	−0.78	84.6745
	EVYQpSIADL	542−550	1117.48130	559.24424	2	−0.08	74.6395
	EVYQpSIADLAVGAKDQAVF	542−560	2103.99983	1052.50322	2	−0.32	91.9885
	QpSIADL	545−550	726.30696	726.30740	1	0.6	51.1828
	QpSIADLAVGAKDQAVF	545−560	1712.82549	856.91466	2	−2.02	76.7837
S565	CEVpSDENVR	562−570	1187.43984	594.22253	2	−1.73	20.8818
S589	IKVpSHIGR	586−593	989.52919	495.26789	2	−0.7	18.0036
T603	LTIDDVpTPADEADYSFVPEGFACNLSAK	597−624	3125.36970	1042.45863	3	−2.68	98.0686
	VHKLTIDDVpTPADEADYSFVPEGFACNLSAK	594−624	3489.59199	1163.87176	3	2.51	81.6246
T603/ S611	VHKLTIDDVpTPADEADYpSFVPEGFACNLSAK	594−624	3569.55832	1190.52603	3	1.46	87.0161
S650	IHLDCPGpSTPDTIVVVTGNK	643−662	2203.04646	735.02074	3	0.55	62.7145
S670	RLDVPIpSGDPAPTVVW	664−679	1801.88843	901.44765	2	−0.22	88.1645
T676	RLDVPISGDPAPpTVVW	664−679	1801.88843	901.44765	2	2.32	43.4000
	LRLDVPISGDPAPpTVVWQK	663−681	2171.12603	724.38000	3	0.96	77.6799
	LDVPISGDPAPpTVVWQK	665−681	1901.94086	951.47300	2	−1.12	78.5432
T682	LRLDVPISGDPAPTVVWQKpTVTQGK	663−687	2785.46481	929.15801	3	−1.92	70.6261
	LDVPISGDPAPTVVWQKpTVTQGK	665−687	2516.27963	839.43192	3	0.63	69.5547
S690	QKTVTQGKKApSAGPHPDAPEDAGADEEW	680−707	3000.33710	1000.78296	3	−0.93	34.2941
	KApSAGPHPDAPEDAGADEEWVFDK	688−711	2619.10352	873.70460	3	−1.63	56.7572
	KApSAGPHPDAPEDAGADEEWVFDKK	688−712	2747.19848	687.55546	4	0.55	48.9652
	ApSAGPHPDAPEDAGADEEWVFDK	689−711	2491.00855	831.00814	3	0.53	64.3351
T717	LLCEpTEGRVR	713−722	1312.60791	656.80736	2	−0.36	27.2343
S730	DRpSVFTVEGAEKEDEGVYTVTVK	728−750	2638.22838	880.08273	3	1.99	62.1456
T733	SVFpTVEGAEKEDEGVYTVTVK	730−750	2367.10033	789.70401	3	−1.21	68.0653

[a]A total of 26 unique phosphopeptides were identified. The sequence numbering is based on the reference sequence UniProtKB O70468. The T603 (LTI···SAK) peptide was found twice, so the Δ*m* and retention times from the first experiment are reported. The second experiment showed the same values except for a Δ*m* of −3.74 ppm and 90.9 min retention time. T676 (RLDVPISGDPAPpTVVW) peptide retention time is from the PRM analysis, and the chromatography for this experiment is shorter than the data-dependent acquisition (DDA) analysis. Mo indicates oxidized methionine, which adds ∼16 Da. Because we reduce and alkylate with iodoacetamide in our protein samples, carbamidomethyl groups (∼57 Da) are added on peptides containing cysteine residues. [M + H] indicates the peptide mass. *m*/*z* indicates mass to charge ratio or observed mass. z indicates charge. Δ*m* (ppm) is the deviation of the observed mass from the theoretical mass of the peptide. ppm indicates parts per million.

https://doi.org/10.1021/acsomega.2c00799
ACS Omega 2022, 7, 14189−14202

Table 2. All 18 Known Phosphorylation Sites in the C4C5 Domains of cMyBPC[a]

	human		mouse		
domain	site	reference	site	reference	overall count
C4	Y548	Schumacher et al., 2007[45]	Y544	Lundby et al., 2013[47]	1
	S550	PhosphoSitePlus[46]	S546	Huttlin et al., 2010,[48] Lundby et al., 2013,[47] this study	2
	S569		S565	this study	3
	S588	PhosphoSitePlus[46]	**N584**		4
	S593		S589	this study	5
	T602	Kooij et al., 2013[25]	T598		6
	T607	Kooij et al., 2013[25]	T603	Lundby et al., 2013,[47] this study	7
	S615		S611	this study	8
C5	**R654**		S650	this study	9
	S674		S670	this study	10
	T680		T676	this study	11
	A686		T682$^{(loop)}$	this study	12
	P694		S690$^{(loop)}$	Huttlin et al., 2010,[48] this study	13
	A695		A/T691#$^{(loop)}$	Huttlin et al., 2010[48]	14
	T708*	Kooij et al., 2013[25]	**D704**		15
	T721		T717	This study	16
	S734		S730	This study	17
	T737		T733	This study	18

[a]Mouse residue numbers of Lundby et al., 2013[47] and our study are from the reference sequence UniProtKB O70468, and human residue numbers of the Kooij et al., 2013[25] study are from the reference sequence UniProtKB Q14896. The sources of the reference sequence for Huttlin et al., 2010,[48] Schumacher et al., 2007,[45] and PhosphoSitePlus v.6.6.0.2[46] could not be confirmed. Bold font indicates that the residue is not conserved compared to the other species. $^{(loop)}$ indicates that these phosphorylation sites are in or near the cardiac-specific loop region of the C5 domain. # indicates that residue 691 is a threonine in the reference sequence NP_032679.2, but it is an alanine residue in the sequence used in our study. There are no known phosphorylation sites on the linker between C4 and C5 domains.

Liquid Chromatography with Tandem Mass Spectrometry (LC-MS/MS). Six kinase-treated and six control bands were washed. Then half of each sample was digested with trypsin, and the other half was digested with chymotrypsin. All of the digests were analyzed by capillary column LC-MS/MS (Figure S4), and the tryptic data was searched against the *E. coli* UniProtKB database that also contained the sequence of the expressed form of the C4C5 fragment of mouse MyBPC (Table S4). These searches confirmed the C4C5 fragment of cMyBPC as the most abundant component of these samples. A range of 4−90 *E. coli* proteins were also identified, and the most abundant *E. coli* protein was identified as FKBP-type peptidyl-prolyl cis−trans isomerase SlyD (5−7 peptides covering 42−69% of the protein sequence). For the identification of PTMs, the data from the tryptic and chymotryptic digests were searched specifically against the sequence of the C4C5 fragment of cMyBPC and 100% of the protein sequence was positively identified. The specific numbers of identified tryptic and chymotryptic peptides of the C4C5 domains, *E. coli* proteins and their respective sequence coverage are summarized in the Table S4.

Identification of Specific Phosphorylated Residues. The data from the trypsin and chymotrypsin digests were searched considering phosphorylation at serine (S), threonine (T), and tyrosine (Y) residues as a variable modification. For enhanced clarity, "human" designation (h) is made after any residue numbers derived from the human cMyBPC sequence (UniProtKB Q14896. or NP_032679.2). From our study, 26 unique phosphorylated peptides with 13 different phosphorylation sites were identified (Table 1). The 8 phosphorylation sites that were previously identified in the C4C5 domains are summarized, along with our findings, in Table 2 to facilitate their comparison.[25,45−48] Phosphorylation sites that are not conserved between human and mouse are shaded in gray (Table 2). From our mass spectrometry results, we confirmed phosphorylation at S546, T603, and S690 but did not identify phosphorylation on the Y544 and T602 (h) sites. We were unable to confirm phosphorylation on S588 (h), T708 (h), or T691 as these sites did not have conserved amino acids. We identified 10 additional phosphorylation sites that have not been characterized in the literature and appear to be novel. These include S565, S589, S611, S650, S670, T676, T682, T717, S730, and T733 (Table 1). No phosphorylation sites were found in the linker region. However, T682 and S690 sites were near or in the cardiac-specific C5 loop region.

These novel phosphorylation sites are scattered throughout the C4C5 domains with three located in the C4 domain and seven in the C5 domain (in addition to the previously known sites S546 and T603 in C4 and S690 in C5). Each of the representative unique phosphopeptides and all of their CID spectra were manually validated for their sequence and phosphorylation status (Figure S5). RSK2 phosphorylated 12 of 13 sites; PKA, AMPK, and PKG1 each phosphorylated 11 of 13 sites; PKD2 phosphorylated 8 of 13 sites; and CK2 phosphorylated 4 of 13 sites. The XCorr scores for each of the peptides and kinases are given in Table S5[49]

Parallel Reaction Monitoring (PRM) Experiments. The degree of phosphorylation at each site can be used as a measure of kinase specificity. The relative abundance of phosphopeptides was determined by performing targeted PRM experiments (Figure S6, Table S6). The presence of phosphopeptides in the control samples may be attributable to endogenous kinases in the bacterial system;[50,51] however, the relative abundance of those peptides are very low. All peptides presented in Table 1 were targeted in this analysis. Chromatograms for the phosphorylated and unmodified forms of each peptide were plotted for each kinase- and control-treated sample, and the relative abundance of each peptide was

https://doi.org/10.1021/acsomega.2c00799
ACS Omega 2022, 7, 14189−14202

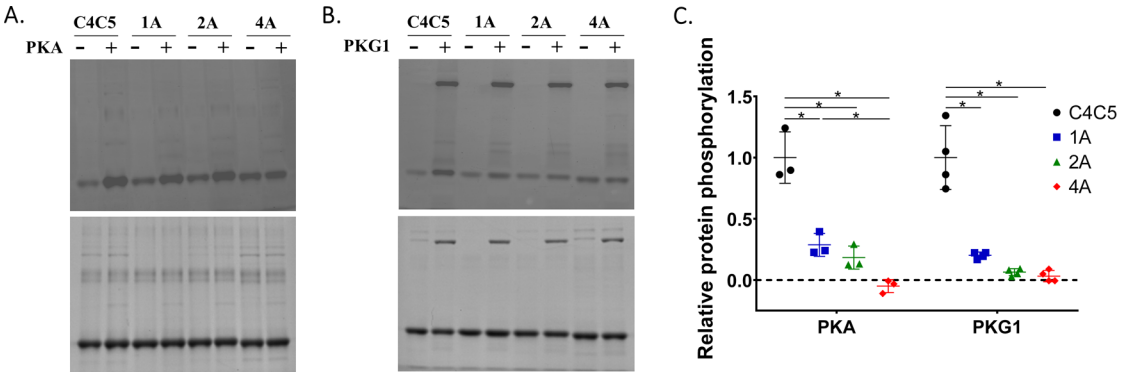

Figure 3. (A) Phospho-stain (top) and coomassie (bottom) of control and PKA-treated C4C5, 1A, 2A, and 4A recombinant proteins. (B) Phospho-stain (top) and coomassie (bottom) of control and PKG1-treated C4C5, 1A, 2A, and 4A recombinant proteins. Pro-Q Diamond Phosphoprotein Gel Stain from Invitrogen was used for these experiments. (C) Scatter plot of normalized relative protein phosphorylation of C4C5, 1A, 2A, and 4A constructs after a 6 h incubation with PKA and PKG1 (n = 3−4). Values are expressed as mean ± SD. Significance was determined by one-way ANOVA with Tukey's multiple comparisons test. * $p < 0.05$ versus C4C5 group.

determined by calculating the peak area (PA) ratios: $PA_{phosphorylated\ peptide}/(PA_{phosphorylated\ peptide} + PA_{unmodified\ peptide})$ (Table S7). Because of the differences between ionization efficiencies of the unmodified and phosphorylated peptides, as well as digestion patterns between the kinase- and control-treated samples, the PA ratios were used only as an estimate, not an absolute measurement, of phosphorylation. In our gross screening comparisons of the abundances of different peptides, the PA ratios were used to identify post-translational alterations that had a large magnitude of change. Most peptides phosphorylated by PKD2 and CK2 were in very low abundance (Table S7). However, PKA-targeted phosphorylation of S690 and S546, as well as the PKG1-targeted phosphorylation of S589 and S690 showed the highest PA ratios among any kinase-site pairs (Table S7). Since PKA and PKG1 are known to be physiologically important, we sought to study them in more detail.[24,25,33,43,52] To this end, four sites (S690, S589, S546, and S730) were selected for further analysis.

C4C5 Phospho Mutant Experiments Using PKA and PKG1. Three C4C5 phospho-ablated mutant constructs with 1A (S690A), 2A (S690A and S589A), and 4A (S690A, S589A, S546A, and S730A) substitutions were generated. They were purified (>90−95% purity), confirmed to be well-structured and folded properly via circular dichroism (Figure S3, Table S1), and incubated with PKA and PKG1. In order to determine the contributions of each site, normalized ratios of kinase-treated to control sample of each protein construct (C4C5, 1A, 2A, and 4A) were calculated and compared using a one-way ANOVA followed by a Tukey's pairwise multiple comparison test (Figure 3). The PKA results showed the largest decline in the normalized relative phosphorylation level in the 1A (0.29 ± 0.09) vs C4C5 construct (1.00 ± 0.21), signifying that the single S690A mutation ablated most of the phosphorylation induced by PKA. Although the individual ablations at site S589 or combined sites S546/S730 did not reach statistical significance (1A vs 2A and 2A vs 4A, ns for both), the ablation of all three sites together significantly reduced phosphorylation levels from the baseline (0.29 ± 0.09 for 1A vs −0.05 ± 0.05 for 4A, $p < 0.05$). In the PKG1-treated samples, an even greater decline in the relative protein phosphorylation level in the 1A vs C4C5 construct was seen (0.20 ± 0.03 for 1A vs 1.00 ± 0.26 for C4C5, $p < 0.05$), indicating that the S690A mutation ablated ∼80% of the PKG1-induced phosphorylation in the C4C5 domains. Additional ablations at S589, S546/S730, or a combination of all three did not yield statistically significant decreases in phosphorylation (Figure 3C).

While there may be many potential phosphorylatable sites in the C4C5 domains, the predominant PKA-induced C4C5 phosphorylation seems to be from S690 (∼71%), with minor contirbutions from the combined phosphorylation at S589, S546, and S730 sites (∼29%). Furthermore, ∼80% of PKG1-induced C4C5 phosphorylation seems to be at the site S690. It is notable that the predominant site of PKA- and PKG1-induced phosphorylation is S690, located in the cardiac-specific loop region (VTQGKKASAGPHPDAPEDAG-ADEEWVFD, UniProtKB O70468).

Although this major site of PKA and PRKG1 induced phosphorylation in the mouse is not conserved with the human sequence (ITQGNKAPARPAPDAPEDTGDSDEWVFD, NP_000247.2), the sequence of the C5 domain's loop region in the mouse is fairly similar to that of the human, with 68% sequence identity. Therefore, the phosphorylation at S690 still likely has relevance and importance in human paysiology and pathophysiology. In fact, the loop region in the human contains S708 (h), which was found to be phosphorylated in patients with end-stage heart failure, but not in heart samples from healthy donors.[25] Although there is mounting evidence that there is an overall decrease in phosphorylation of cMyBPC in heart failure,[22] it seems plausible that dysregulated and abnormal phosphorylation of cMyBPC could also contribute to the disease state. In this case, a phosphorylation event of the S690 site in mouse may serve the same purpose as the S708 site in human.

Additional Post-Translational (PTM) Modification Analysis. In addition to phosphorylation sites on C4C5, the LC-MS/MS results were also searched for carbamidomethylation (oxidation) at M (methionine), acetylation at K (lysine), citrullination at R (arginine), ubiquitination at K, and methylation at K and R as variable modifications. This search resulted in 8 unique acetylated peptides and 12 unique ubiquitinated peptides, representing 6 acetylation and 11 ubiquitination sites in the C4C5 domains (Table S8). From our C4C5 samples, citrullination and methylation at K and R were not found. Although there have been reports of acetylation of recombinant cMyBPC, most of the identified sites are localized in the N-terminal domains and none have

https://doi.org/10.1021/acsomega.2c00799
ACS Omega 2022, 7, 14189−14202

been found in the central domains of C4 and C5.[7,53] Therefore, all 6 acetylation sites that were found in the C4C5 domains in this study seem to be novel (K540, K555, K561, K662, K681, and K711).

The PhosphoSitePlus database showed that there are six known ubiquitination sites in and near the C4C5 domains (K539-not in our construct but adjacent to the C4 domain, K540, K561, K688, K711, and K712).[46,54] From our LC-MS/MS search, we were able to detect four of the previously known sites (K540, K561, K688, and K712), while the remaining seven sites appear to be novel (K555, K575, K578, K596, K662, K681, and K739). As a comprehensive summary, all known acetylation and ubiquitination sites in C4C5 are listed in Table 3. The functions of these interesting PTMs are

Table 3. All Known Acetylation and Ubiquitination Sites in the C4C5 Domains of Mouse cMyBPC[a]

domain	site	references
	Acetylation	
C4	K540	this study
	K555	this study
	K561	this study
C5	K662	this study
	K681$^{(loop)}$	this study
	K711$^{(loop)}$	this study
	Ubiquitination	
C4	(K539)	Wagner et al., 2012[54]
	K540	Wagner et al., 2012,[54] this study
	K555	this study
	K561	Wagner et al., 2012,[54] this study
	K575	this study
	K578	this study
	K596	this study
C5	K662	this study
	K681$^{(loop)}$	this study
	K688$^{(loop)}$	Wagner et al., 2012,[54] this study
	K711$^{(loop)}$	Wagner et al., 2012[54]
	K712$^{(loop)}$	Wagner et al., 2012,[54] this study
	K739	this study

[a]No acetylation sites were found in the C4C5 domains of human cMyBPC based on PhosphoSitePlus v.6.6.0.2.[46] Some ubiquitination sites on C4C5 domains were previously described by Wagner et al., 2012.[54] Although the Ub-K539 site was not included in the C4 domain as per our domain definition, we included it in this summary because of its proximity to the C4 domain. $^{(loop)}$ indicates that the site is in or near the C5 loop. In summary, there are 6 unique acetylation sites and 13 unique ubiquitination sites in C4C5 domains.

not yet known, and more studies are necessary to elucidate their importance. Each of the representative unique acetylated and ubiquitinated peptides and their CID spectra were manually validated (Figure S7).

Hypothesized Role of Phosphorylation and Other PTMs in the C4C5 Domains. The extensive research on the N-terminal C0C2 domains of cMyBPC supports the idea that phosphorylation of the M-domain of cMyBPC is crucial for cardiac contractile function and overall cardiac health. cMyBPC phosphorylation facilitates actin−myosin interactions and cross bridge kinetics by modulating the stability and extensibility of the N-terminal domains.[6,29,55,56] Specifically, phosphorylation of the M-domain is thought to release myosin heads from their interacting heads motif (IHM) or the super-relaxed (SRX) state, aiding in the transition to the force generating state.[57−60]

Our study and others have increasingly shown that there may be other sites of important functional regulation, such as the C4C5 domains. Most notably, the central region of cMyBPC, including the C4 and C5 domains, is thought to interact with IHM/proximal myosin S2 and be partly responsible for maintaining myosin's SRX state.[58,61] The N-terminal domains of cMyBPC are biased toward the actin filaments in situ and may not lie along the surface of the thick filament.[61−63] Thus, these data imply that the central domains may be responsible for, or at least aid in, stabilizing the SRX state, if resulting from the IHM. Additionally, a recent study utilizing microscale thermophoresis demonstrated that high affinity interaction sites of myosin S1 are localized to the cMyBPC central domains.[32] Based on this finding, it seems plausible that the central domains can play a central role in modulating the SRX. Furthermore, phosphorylation of those central domains could provide an additional layer of regulation of cross bridge activation, potentially by releasing myosin molecules from the IHM or the SRX state. We found that the novel S690 site is targeted by potent and established regulators of cMyBPC such as PKA and PKG1, which may underlie the molecular basis for the changes observed in the SRX state.[57,64]

Other diverse PTMs in the C4C5 domains have been found to regulate cMyBPC function. For example, it has been shown that in vitro S-glutathionylation of cMyBPC at C627 and C655 (NP 032679.2) is correlated with increased myofilament Ca^{2+} sensitivity, slowing of cross-bridge kinetics, and diastolic dysfunction.[65,66] In addition, the residue R696 in humans undergoes citrullination associated with protein dysfunction and cardiovascular disease.[67] R696 is located in the cardiac-specific C5 loop region but is not conserved among either of the two mouse sequences. Furthermore, the acetylation and ubiquitination sites found in this study suggest that C4C5 may play a role in cMyBPC proteolysis and degradation (Table 3, Table S8).[7,54,68] Thus, there is evidence that the C4C5 domains may be essential in integrating multiple PTM signals and aiding in regulation of the downstream function of cMyBPC.[69] We speculate that these PTMs of cMyBPC provide regulatory pathways that alter cardiac function when activated in response to physiological and pathological stress conditions. The physiological significance of our in vitro results will need to be confirmed in in vivo settings. All known phosphorylation, acetylation, and ubiquitination sites on the C4C5 domains of mouse cMyBPC are listed in Table 2 and Table 3, and a combined landscape of those three PTMs are summarized in Figure 4.

CONCLUSIONS

This study characterized the phosphorylation, acetylation, and ubiquitination sites in the C4 and C5 domains of mouse cMyBPC. Our LC-MS/MS identified 10 novel phosphorylation sites, 6 novel acetylation sites, and 7 novel ubiquitination sites on C4C5 (Table 1, Table S8). Many of the phosphorylation sites identified were targeted by different kinases (Table S7), but the mouse S690 site seemed to be the primary target of both PKA and PKG1 (Figure 3). Additionally, the presence of many of the PTMs in the cardiac-specific loop of the C5 domain suggests that the loop could play an important role in functional regulation.

https://doi.org/10.1021/acsomega.2c00799
ACS Omega 2022, 7, 14189−14202

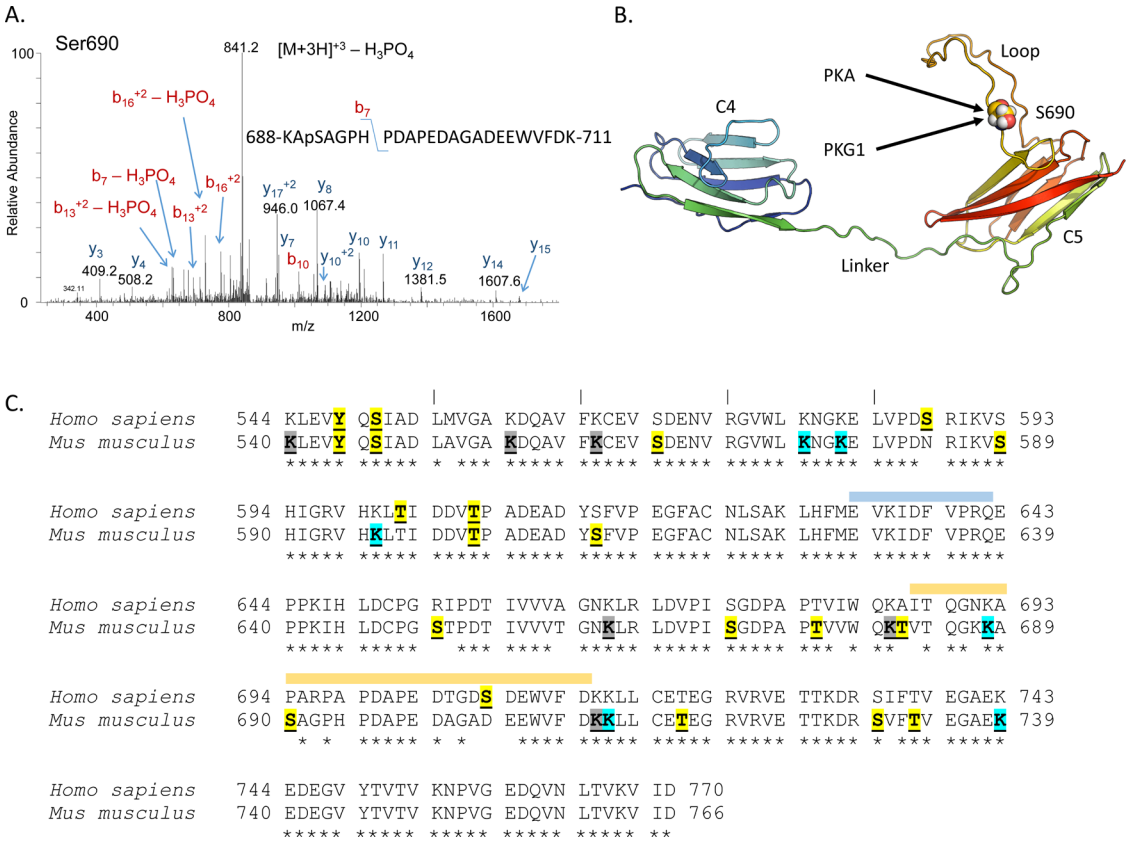

Figure 4. Summary of the phosphorylation, acetylation, and ubiquitination landscape in the C4C5 domains of cMyBPC. (A) Collision-induced dissociation (CID) spectra of a representative modified peptide containing the S690 phosphorylation site. A triply charged peptide with a mass of 873.704 Da was identified in the tryptic digest of C4C5 and is within −1.63 ppm of the expected mass for the KASAGPHPDAPEDAGADE-EWVFDK + PO_3 peptide. The CID spectra for this peptide contains several C-terminal y ions and the masses of these ions are consistent with the modification at S690. (B) A molecular model of the C4C5 domains of mouse cMyBPC is shown with the S690 site and the kinases (PKA and PKG1) targeting that site. Although the S589, S546, and S730 sites were also targeted by PKA, they are not represented in the model because of their low contribution to the overall phosphorylation of C4C5. Linker and loop regions are labeled. (C) A sequence alignment of the C4C5 domains of human and mouse cMyBPC (UniProtKB Q14896 and O70468) with all known phosphorylation (18), acetylation (6), and ubiquitination (13) sites in the C4 and C5 domains, excluding a nearby ubiquitination site at K539 (Wagner et al., 2012[54]). The C4 domain is defined as residues K540 to M628 and the C5 domain is defined as residues E639 to D766 in this study. Note that although residue 691 is an alanine from our reference sequence, Huttlin et al., 2010[48] reported T691 phosphorylation in the reference sequence NP_032679.2. All PTMs are bolded and underlined. Phosphorylation, acetylation, and ubiquitination sites are color coded as yellow, red, and blue, respectively. The sites targeted by both acetylation and ubiquitination are highlighted gray. All six acetylated site were shared sites for ubiquitination, so red was not used in the figure. From this study, 10 phosphorylation, 6 acetylation, and 7 ubiquitination sites found seem to be novel. The blue and orange shaded areas represent the linker and the loop regions, respectively. * indicates sequence identity.

LIMITATIONS

Although steps were taken to minimize the limitations of our study, there are a few worth mentioning. First, we prioritized kinases that are known to be physiologically important and/or have been shown to target MyBPC; however, it is possible that we did not study all of the relevant kinases. For example, although GSK3β has been implicated in MyBPC phosphorylation, we were not able to obtain this kinase for the study.[70] In addition, the long incubation times used to attempt maximal phosphorylation of the substrates by kinases such as PKCα may not be physiological. Although the sequence of mouse and human cMyBPC in the C4C5 domains are quite similar (~92% identical), the differences may confer different kinase specificity for phosphorylation. It is possible that in our bottom-up LC-MS/MS analysis, the peptides containing the PTMs may have been lost during the separation step, leading to underestimation of the abundance of those peptides.[71] Lastly, the functional roles of the PTMs in vivo and the interactions that they have with each other will require further study.

METHODS

Transgenic Animals and Ethical Approval. Non-transgenic wild type (WT) mice with 129/Sv background expressing full-length cMyBPC, cMyBPC knockout (KO) mice, and transgenic mice expressing nonphosphorylatable cMyBPC with serine to alanine substitutions at 273, 282, and 302 residues (ie, 3SA) were used in this study.[9,72] cMyBPC 3SA mice were generated on the same KO background to eliminate endogenous phosphorylation of the three aforementioned sites. Mice, aged 6 to 9 months old, of both sexes were used for WT, KO, and 3SA hearts in this study. All procedures involving animal care and handling were reviewed and approved by the Case Western Reserve University Animal Care and Use Committee.

AAV9 Production and Administration. AAV9 pseudotyped vectors expressing full-length murine cMyBPC (KO^{FL})

https://doi.org/10.1021/acsomega.2c00799
ACS Omega 2022, 7, 14189−14202

and full-length murine cMyBPC with Ser-to-Ala substitutions at sites 273, 282, 302, and 307 (4SA) were designed under the control of a truncated chicken cardiac troponin T (cTnT) promoter, which confers cardiac specificity to gene expression.[73] Additionally, a c-Myc tag was included at the c-terminus, i.e. pENN.AAV.cTNT.mMyBPC3 (KO^{FL} or 4SA)-cMyc.bGH. Vectors were produced by the Penn Vector Core, Gene Therapy Program at the University of Pennsylvania (Philadelphia, Pennsylvania, U.S.A.), as described previously.[13,74] In short, the AAV vectors were generated by triple transfection using (1) an AAV cis plasmid carrying a transgene expression cassette flanked by the viral inverted terminal repeats (ITRs), (2) an AAV trans plasmid encoding the AAV2 replicase and AAV9 capsid genes, and (3) a plasmid encoding adenoviral genes providing helper functions for AAV replication. HEK293 cells (American Type Culture Collection [ATCC], Manassas, VA) were grown in 10-layered cell factories and transfected using PEI-Max (Polysciences, Warrington, PA). The vectors were purified from culture media as described.[74] The specific murine KO^{FL} and 4SA sequences used in this study are listed in Figure S1. Because of the usage of an early mouse cMyBPC cDNA sequence (i.e., NM_008653.1), the KO^{FL} sequence is identical to NP_032679.2, except that it does not have the eight residue N-terminal extension.[75] Within 36 h of birth, neonatal pups were anesthetized by hypothermia and injected intravenously via the temporal facial vein with 2×10^{11} genome copies (GC) using a 33 gauge needle in standard Biosafety Level 1 (BSL-1) and Animal Biosafety Level 1 (ABSL-1) conditions. Six weeks after the injection, hearts were excised under deep anesthesia and immediately flash frozen and stored at −80 °C until use.

Sample Preparation of WT and 3SA Hearts and FL- and 4SA-Injected Heart Tissue. Myocardial proteins were analyzed as previously described.[13,76] Briefly, hearts were excised from mice anesthetized with 4% isoflurane, flash frozen in liquid N_2, and stored at −80 °C for later use. Sections were taken from the ventricles of frozen hearts. Tissue was thawed in relax solution and then mechanically homogenized. Homogenized myofibrils were skinned for 15 min using 1% Triton X-100 on a mechanical rocker and then centrifuged at 10 000*g* for 5 min. Myofibril pellets were resuspended in fresh relax solution containing protease and phosphatase inhibitors (PhosSTOP and cOmplete ULTRA Tablets; Roche Applied Science, Indianapolis, IN, U.S.A.). Samples were kept on ice throughout the procedure. The protein concentration of each sample was determined by bicinchoninic acid (BCA) protein colorimetric assay (Pierce BCA Protein Assay Kit, Thermo Scientific). Samples were solubilized to a final concentration of 1× laemmli buffer (LB) with β-mercaptoethanol (BME) and 1 μg/μL of protein, heated at 95 °C for 5−10 min, and stored at −20 °C.

Gene Synthesis and Protein Expression. pET-30a(+) plasmid vector carrying DNA fragments of mouse cardiac myosin binding protein C (cMyBPC) C4C5 domains tagged with N-terminal His_6-tags were obtained from GenScript (Piscataway, NJ). The amino acid sequence of the C4C5 recombinant protein along with the three phospho-ablated mutants (1A, 2A, and 4A) are provided in Figure S2. The three C4C5 phospho-ablated mutant constructs have the following substitutions: 1A (S690A), 2A (S690A and S589A), and 4A (S690A, S589A, S546A, and S730A). Because of differences in numbering of the human cMyBPC (NP 000247.2 with 1274 residues) and two different mouse cMyBPC (UniProtKB/SwissProt O70468 with 1270 residues and NP 032679.2 with 1278 residues) sequences in various papers, the reference sequence will be specified as needed. Representative human and mouse C4C5 domains' sequences were aligned and compared using Clustal Omega.[77]

E. coli BL21 Star (DE3) cells were transfected with the above plasmid vectors using heat shock and grown on agar plates. *E. coli* pilot culture was grown in lysogeny broth (LB) - Miller formulation (10 g/L tryptone, 5 g/L yeast extract, 10 g/L NaCl) containing kanamycin (34 μg/mL working concentration) at 37 °C/225 rpm on a MaxQ 4000 Benchtop Orbital Shaker for 16 h. 15% glycerol stocks of each construct were made, flash frozen in liquid N_2, and stored at −80 °C for subsequent steps. The pilot 50 mL culture was diluted into 1 L of the same growth medium and continued to incubate for 3−5 h at 37 °C shaken at 225 rpm until $OD_{600\ nm}$ was approximately 1.0. At that time, the culture was cooled down on ice for 30 min, and 0.5 mM isopropyl β-D-1-thiogalactopyranoside (IPTG) was added. The expression of the recombinant C4C5 was induced overnight at 16 °C with shaking at 225 rpm. The cells were harvested by centrifuging at 6000 rcf at 4 °C for 10 min, and the pellet was resuspended in 25 mL of cold lysis buffer (20 mM HEPES pH 7.5, 500 mM KCl, 10 mM Imidazole, 1 mM 4-(2-aminoethyl) benzenesulfonyl fluoride hydrochloride(AEBSF)), flash frozen in liquid N_2, and stored at −80 °C until purification.

Recombinant Protein Purification. The frozen cells were thawed in RT (∼21 °C) and resuspended in about 50 mL of cold lysis buffer plus a protease tablet (cOmplete ULTRA Tablets, Mini, EDTA-free EASYpack protease inhibitor cocktail, Roche). The cells were lysed with the Avestin Emulsiflex C3 homogenizer (ATA Scientific) at a pressure of 10 000−15 000 psi at 4 °C. The cell homogenates were clarified at 50 000 rpm at 4 °C using the Beckman Coulter Optima L-100 XP Ultracentrifuge with Type 70 Ti Rotor for 1 h. The supernatant was incubated with HisPur Ni-NTA Resin that was prewashed in wash buffer (20 mM HEPES pH 7.5, 500 mM KCl, and 50 mM Imidazole) on a rocker for 2−3 h at 4 °C. Proteins were placed in a 15-mL gravity flow column (Econo-Pac Chromatography Column) and washed with 10−15 mL of wash buffer. The His_6-tagged recombinant proteins were eluted from the column using a total of 4 mL of elution buffer (20 mM HEPES pH 7.5, 500 mM KCl, and 250 mM 250 mM imidazole). Because of the high purity at this stage, all fractions were collected and concentrated using a centrifugal concentrator (Amicon Ultra Centrifugal Filter Unit, 10 kDa molecular weight cut off) according to manufacturer's instructions. The concentration was determined by UV absorbance at 280 nm (A_{280}) using the Beckman Coulter DU 800 Spectrophotometer corrected for background light scattering and the theoretical extinction coefficient calculated from ExPASy ProtParam tool.[78] An appropriate amount of protein sample was injected in the NGC Medium-Pressure Liquid Chromatography System with an ENrich High-Resolution Size Exclusion Column 70 (10 × 300 mm, BioRad) equilibrated in HEPES buffered saline (HBS) (20 mM HEPES pH 7.5, 150 mM NaCl). All fractions containing C4C5 constructs were collected and pooled. The final stock protein concentration was determined by UV absorbance at 280 nm as described above. Purified proteins were >90−95% pure by Coomassie staining. All experiments were done with fresh protein samples within 1 week of purification or immediately after thawing from −80 °C.

https://doi.org/10.1021/acsomega.2c00799
ACS Omega 2022, 7, 14189−14202

Far-UV Circular Dichroism (CD) Spectroscopy. The CD spectra of the C4C5, 1A, 2A, and 4A constructs were recorded on the Jasco J-1500 CD Spectrophotometer with a quartz cuvette with a 0.1 cm path length. The cuvette was cleaned with 2 M nitric acid, rinsed with water, and dried with nitrogen gas after each day of use. All of the proteins were dialyzed in boric acid-sodium fluoride buffer, pH 7.4 (10 mM boric acid, 150 mM NaF). Protein concentrations were determined by UV absorbance at 280 nm with baseline correction at 340 nm via NanoDrop 2000 Spectrophotometer (Thermo Scientific). An initial protein concentration of 0.20 mg/mL was used for all groups, and the exact concentration for MRE calculations was obtained after each trial: 0.161 ± 0.004 mg/mL for C4C5, 0.197 ± 0.14 mg/mL for 1A, 0.209 ± 0.018 for 2A, and 0.205 ± 0.008 for 4A (n = 3 for each). The CD measurements were taken at 37 °C with the following settings: wavelength range of 260−180 nm, bandwidth of 1 nm, step size of 1 nm, averaging time of 5 s, D.I.T. of 2 s, and scanning speed of 100 nm/min. Each experiment consisted of three trials with 3 accumulations each. All accumulations were averaged, and then background corrections were done by subtracting the spectra of the boric acid- NaF buffer. Mean residue ellipticity or $[\theta]_{MRE}$ (deg*cm^2*dmol^{-1}) was calculated using the following formula: $[\theta]_{MRE} = (\theta_{obs} * MRW)/(10 * l * c)$, where θ_{obs} is the raw CD signal in milli-degrees, l is the path length in cm, and c is the concentration in mg/mL. MRW or mean residue weight is $M/(N-1)$, where M is the molecular weight in g/mol, and N is the number of amino acids. No smoothing was necessary. The raw MRE traces were analyzed by BeStSel[79] and CDSSTR (reference set 7) algorithms.[80] The MRE data were averaged together and graphed using GraphPad Prism 6.

In Vitro Kinase Assays of the C4C5 Domains. To study the phosphorylation of the C4C5 protein, the protein was incubated in various kinases per 100 μL incubation volume in 37 °C for 3 and 6 h. The kinases used with their full protein names, gene symbol, manufacturer information, as well as protein substrate:kinase concentration ratios, are shown in Table S2 and Table S3. Control samples were incubated under identical conditions, without the addition of kinase. Briefly, component stocks were mixed sequentially on ice: water, 100 mM adenosine-5′-triphosphate (ATP) pH 7.5 stock, 10× protease and phosphatase inhibitor stock, HBS buffer with 1 mM Dithiothreitol (DTT), and 10× cofactor stocks according to manufacturer's instructions. Final incubation formulation consisted of 1 μg/μL protein, 2 mM ATP pH 7.5, HBS with DTT, 1× protease and phosphatase inhibitor cocktail, and cofactors. After equilibrating each sample tube at 25 °C, C4C5 was put in each tube. Next, each kinase was mixed with the rest of the sample, and transferred to 37 °C. At 3- and 6-h time points, the kinase reactions were terminated by adding 2x LB with BME. The samples were vortexed, heated at 90 °C for 10 min, and stored at −20 °C. For kinase experiments of the phospho-ablation mutants (1A, 2A, and 4A), a similar incubation strategy was used except for a substitution of cyclic guanosine-3′,5′-monophosphate (cGMP) with 100 μM 8-Bromo-cGMP (8Br-cGMP) stock and homemade 3× LB with BME.

SDS-PAGE and Coomassie Staining. For solubilized myofibril samples, 5 μg/lane was loaded on sodium dodecyl sulfate polyacrylamide gel electrophoresis (SDS-PAGE) gels and electrophoretically fractionated using 4−12% TruPAGE Precast Gels (Sigma-Aldrich) at 180 V for 35 min or hand-cast 6% Tris-Glycine gels at 175 V for 50 min. For kinase-treated and control C4C5 samples, 3 μg protein/lane were loaded on 4−12% TruPAGE Precast Gels and separated at 175 V for 45 min. For the phospho-ablation mutant samples (1A, 2A, and 4A), 4−12% TruPAGE Precast Gels at 180 V for 35 min were used.

Total phosphorylation level was measured using Phospho-Tag Phosphoprotein Gel Stain (ABP Biosciences) or Pro-Q Diamond Phosphoprotein Gel Stain (Invitrogen), imaged using the GE Healthcare Typhoon Trio Variable Mode Imager System. For total protein level determination, the gel was counterstained with GelCode Blue Stain Reagent (Thermo Scientific) or a "Blue silver" colloidal Coomassie formulation (10% phosphoric acid, 10% ammonium sulfate, 0.12% G-250 dye, and 20% methanol).[81] Coomassie was imaged using the Azure Biosystems c600 Imaging system. The total phosphorylation levels of myofilament proteins from the phospho-stain densities were normalized to the total protein expression levels from the corresponding density band from the Coomassie stain. The total phosphorylation/total protein ratio of the kinase lane was divided by the total phosphorylation/total protein ratio of the corresponding control lane to obtain the normalized phosphorylation level of the kinase lane. The normalized phosphorylation levels of each kinase were averaged among the n = 3 and n = 4 technical replicates for the 3 and 6 h samples, respectively. Densitometric scanning of stained gels was performed using ImageJ software available from the U.S. National Institutes of Health, Bethesda, MD, U.S.A.[82]

In order to quantify the phosphorylation status of the phospho-ablated mutant C4C5 constructs, the total phosphorylation was first normalized to its total protein as described above. These raw ratios of control and kinase samples were compared using a two-tailed t test. Then, the phosphorylation ratio was normalized to the corresponding control lane that was not incubated with any kinase (ie. phospho kinase-treated/phospho control-treated, double normalized). To compare the contribution of each site to the total kinase-induced phosphorylation level of C4C5, each phospho mutant (1A, 2A, and 4A) was expressed as a percentage of the total C4C5 phosphorylation level (e.g., phospho 1A/phospho C4C5).

Tryptic Digestion. For mass spectrometry analysis, a subset of our kinase and control samples were run on SDS-PAGE, stained with GelCode Blue Stain Reagent (Thermo Scientific), and destained with Milli-Q water overnight as described above. The samples included were those treated with ribosomal protein S6 kinase A3 (RSK2), cAMP dependent protein kinase (PKA), protein kinase cGMP-dependent 1 (PKG1), AMP-activated protein kinase (AMPK), protein kinase D2 (PKD2), and casein kinase 2 (CK2). Each band contained 3 μg of the C4C5 protein. The protein samples were subjected to in-gel digestion. In brief, a small band around the bait protein was cut from the gels, minimizing excess polyacrylamide. These bands were washed in 50% ethanol and 5% acetic acid. For the protein digestion, these bands were divided into a number of smaller pieces. The gel pieces were washed with water, dehydrated in acetonitrile, and dried in a SpeedVac evaporator. The bands were then reduced with DTT and alkylated with iodoacetamide prior to the in-gel digestion. All bands were digested in-gel by adding 5 μL of 10 ng/μL trypsin or chymotrypsin, in 50 mM ammonium bicarbonate, followed by incubation overnight at room temperature. The peptides that were formed were extracted from the polyacrylamide into two aliquots of 30 μL in 50% acetonitrile

https://doi.org/10.1021/acsomega.2c00799
ACS Omega 2022, 7, 14189−14202

and 5% formic acid. These extracts were combined and evaporated to <10 μL in a SpeedVac evaporator and then resuspended in 1% acetic acid to make up a final volume of ∼30 μL for LC-MS/MS analysis. No tryptic phosphopeptide enrichment was done.

Liquid Chromatography with Tandem Mass Spectrometry (LC-MS/MS) and Parallel Reaction Monitoring (PRM) Experiments. The LC-MS/MS system was a Thermo Scientific Finnigan LTQ Obitrap Elite hybrid mass spectrometer system or the Thermo Scientific Orbitrap Fusion Lumos Tribrid mass spectrometer system, coupled with the Dionex UltiMate 3000 nanoflow HPLC. The HPLC system used the Thermo Scientific Acclaim PepMap 100 trapping precolumn cat. no. 164564 (100 μm internal diameter × 2 cm column length, C18 stationary phase, 5 μm particle size, 100 Å pore size) followed by the Acclaim PepMap100 analytical column cat. no. 164569 (75 μm i.d. × 25 cm, C18, 3 μm, 100 Å). 5 μL volumes of the extract were injected, and the peptides eluted from the column in an acetonitrile/0.1% formic acid gradient at a flow rate of 0.3 μL/min were introduced into the source of the mass spectrometer online. The microelectrospray ion source was operated at 1.9 kV.

The digest was analyzed in both a survey manner and a targeted parallel reaction monitoring (PRM) manner. The survey experiments were performed using the data-dependent multitask capability of the instrument acquiring full scan mass spectra to determine peptide molecular weights and product ion spectra to determine amino acid sequence in successive instrument scans. For the Orbitrap Elite experiments, MS1 scans were taken in the Orbitrap at a resolution of 60 000, and a top 10 data-dependent strategy was used for MS/MS analysis which was performed by collision induced dissociation (CID) and detected in the ion trap. For the Lumos experiments, MS1 scans were taken in the Orbitrap at a resolution of 120 000, and a 3-s cycle time was used for MS/MS analysis, which was performed by CID and detected in the ion trap.

The LC-MS/MS data searches were performed, utilizing the program Sequest bundled into Proteome Discoverer v2.3, against the full *E. coli* BL21 UniProtKB database (downloaded in April 2021, 4156 entries) and specifically against the sequence of the recombinant mouse C4C5 domains of cMyBPC. The parameters used in these searches include 10 ppm MS1 (peptide) mass tolerance, 0.6 Da MS/MS (fragment ion) mass tolerance, full and semiprotease specificity for trypsin and chymotrypsin, respectively, with 3 and 4 missed cleavages for trypsin and chymotrypsin, respectively. For all searches, carbamidomethylation of cysteine was considered a static modification; the oxidation of methionine, phosphorylation at serine, threonine, and tyrosine, acetylation at lysine (K), citrullination at arginine (R), ubiquitination at K, and methylation at K and R were considered as variable or dynamic modifications. The *E. coli* database search results were filtered using the Percolator node in Proteome Discoverer to a peptide- and protein-level FDR rate <1% using a target decoy strategy, and at least three peptides were required for protein identification. For specific searches for the C4C5 domains of cMyBPC, the Fixed Value PSM validator node was used. All positively identified modified peptides were manually inspected and validated to have a monoisotopic mass <5 ppm of theoretical mass, comprised of a majority of major ions mapped to either y or b ions, and contain ions that are consistent with the identified modification.

The PRM experiments involve the analysis of specific cMyBPC peptides including the phosphorylated and unmodified forms of several tryptic and chymotryptic peptides.[83,84] The chromatograms for these peptides were plotted based on known fragmentation patterns and the peak areas of these chromatograms were used to determine the extent of phosphorylation.

C4C5 Molecular Modeling and Figure Rendering. In order to create a C4C5 model, a literature search of the Protein Data Bank (PDB) was done,[85] and available experimental structures were identified: 2DLT (mouse, fast isoform, DOI 10.2210/pdb 2DLT/pdb) and 2YUZ (human, slow isoform, DOI 10.2210/pdb 2YUZ/pdb) for the C4 domain and 1GXE[31] (human, cardiac isoform, DOI 10.2210/pdb 1GXE/pdb) for the C5 domain. The most representative NMR models of 2DLT and 1GXE (model 2 for both) were selected for further modeling using an analysis of NMR structure ensembles (OLDERADO).[86] Template-based homology modeling of the mouse cMyBPC C4 and C5 domains were done with the I-TASSER server[87] using the mouse cMyBPC sequence (UniProtKB Accession No. O70468). The specific amino acids used in the modeling process were identical to the recombinant protein constructs without the N-terminal methionine and His_6-tags. The C4 and C5 domains were separated and iteratively refined using locPREFMD,[88] Galaxy WEB,[89] and MolProbity[90] to reduce steric clashes and to improve protein geometry and global/local conformations. The linker region between C4 and C5 was also modeled using I-TASSER and refined as described above. In order to connect the C4 and C5 domains through the linker region, the overlapping regions of C4 domain/linker and linker/C5 domain were aligned with each other. Then, the linker peptide was truncated and each side of the truncated linker peptide was manually connected using the "bond" command in The PyMOL Molecular Graphics System (version 2.4.1. Schrödinger, LLC). Molecular models and related images were rendered using PyMOL

Data and Statistical Analysis. Comparisons of protein phosphorylation levels for the 3SA and 4SA samples were performed using a two-tailed *t* test. Comparisons of secondary structures were performed using a one-way ANOVA followed by the Dunnett multiple comparison test. Comparisons of different groups in the phospho mutant measurements were performed using a one-way ANOVA followed by a post hoc Tukey's multiple comparison test. Values are reported as mean ± standard deviation (SD) unless mentioned otherwise. The criterion for statistical significance was set at $p < 0.05$. All statistical analysis were performed using GraphPad Prism Software version 6.01, La Jolla California U.S.A., www.graphpad.com.

■ ASSOCIATED CONTENT

Supporting Information

The Supporting Information is available free of charge at https://pubs.acs.org/doi/10.1021/acsomega.2c00799.

Murine cMyBPC full length and 4SA DNA and amino acid sequences and alignment; amino acid sequences of C4C5 recombinant proteins; far-UV circular dichroism spectra of C4C5, 1A, 2A, and 4A; total ion chromatograms; collision induced dissociation spectra of phosphopeptides; targeted parallel reaction monitoring experiments of phosphopeptides; CID spectra of

https://doi.org/10.1021/acsomega.2c00799
ACS Omega 2022, 7, 14189−14202

ubiquitinated and acetylated peptides; secondary structure quantification via CDSSTR and BeStSel algorithms; information on the kinases used in the study; protein substrate:kinase concentration ratios used in kinase experiments; summary of peptides and sequence coverage from mass spectrometry; XCorr values from the phosphopeptide search; summary of PRM transitions of phosphopeptides; peak area ratios calculated from PRM experiments; and acetylated and ubiquitinated peptides identified in the LC-MS/MS analysis (PDF)

AUTHOR INFORMATION

Corresponding Author

Julian E. Stelzer − *Department of Physiology and Biophysics, School of Medicine, Case Western Reserve University, Cleveland, Ohio 44106, United States*; Phone: (216) 368-8636; Email: julian.stelzer@case.edu; Fax: (216) 368-5586

Authors

Chang Yoon Doh − *Department of Physiology and Biophysics, School of Medicine, Case Western Reserve University, Cleveland, Ohio 44106, United States*; orcid.org/0000-0002-5071-4832

Katherine L. Dominic − *Department of Physiology and Biophysics, School of Medicine, Case Western Reserve University, Cleveland, Ohio 44106, United States*; orcid.org/0000-0002-9359-2871

Caitlin E. Swanberg − *Department of Physiology and Biophysics, School of Medicine, Case Western Reserve University, Cleveland, Ohio 44106, United States*

Nikhil Bharambe − *Department of Physiology and Biophysics, School of Medicine, Case Western Reserve University, Cleveland, Ohio 44106, United States*

Belinda B. Willard − *Proteomics and Metabolomics Laboratory, Lerner Research Institute, The Cleveland Clinic Foundation, Cleveland, Ohio 44195, United States*

Ling Li − *Proteomics and Metabolomics Laboratory, Lerner Research Institute, The Cleveland Clinic Foundation, Cleveland, Ohio 44195, United States*

Rajesh Ramachandran − *Department of Physiology and Biophysics, School of Medicine, Case Western Reserve University, Cleveland, Ohio 44106, United States*

Complete contact information is available at: https://pubs.acs.org/10.1021/acsomega.2c00799

Author Contributions

The manuscript was written through contributions of all authors. C.Y.D., B.B.W., and J.E.S. contributed to the conception and design of the experiments. C.Y.D., K.L.D., C.E.S., N.B., B.B.W., and L.L. participated in performing the experiments and data acquisition. C.Y.D., B.B.W., R.R., and J.E.S. participated in data analysis, data interpretation, and drafting the manuscript. All authors participated in revising the manuscript and given approval to the final version of the manuscript.

Funding

The Orbitrap Elite and Fusion Lumos LC-MS/MS instruments were purchased via shared instrument grants from the NIH National Center for Research Resources (NCRR) (S10 RR031537) and NIH Office of the Director (OD) (S10 OD023436), respectively. This work was also supported by the NIH National Institute of General Medical Sciences (NIGMS) grant R01 GM121583 and NIH National Heart, Lung, and Blood Institute (NHLBI) grants R01 HL146676 and R01 HL114770.

Notes

The authors declare no competing financial interest.

The mass spectrometry proteomics data have been deposited to the ProteomeXchange Consortium via the PRIDE partner repository[91,92] with the data set identifier PXD031262 and 10.6019/PXD031262. All other data are available from the corresponding author upon request.

ACKNOWLEDGMENTS

We thank the Penn Vector Core, Gene Therapy Program at the University of Pennsylvania for providing the gene vectors and assisting in the design and production of the AAV9 used in this study. We thank Dr. Yinghua Chen for circular dichroism measurements from the PEPCMBC facility in the Department of Physiology and Biophysics, Case Western Reserve University. We thank Dr. Susan C Wang (Case Western Reserve University) for providing advice on molecular biology techniques and mass spectrometry.

ABBREVIATIONS

cMyBPC, cardiac myosin binding protein C; PTMs, post-translational modifications

REFERENCES

(1) Flashman, E.; Redwood, C.; Moolman-Smook, J.; Watkins, H. Cardiac Myosin Binding Protein C: Its Role in Physiology and Disease. *Circ. Res.* **2004**, *94* (10), 1279−1289.

(2) Heling, L. W. H. J.; Geeves, M. A.; Kad, N. M. MyBP-C: One Protein to Govern Them All. *J. Muscle Res. Cell Motil.* **2020**, *41* (1), 91−101.

(3) Gautel, M.; Zuffardi, O.; Freiburg, A.; Labeit, S. Phosphorylation Switches Specific for the Cardiac Isoform of Myosin Binding Protein-C: A Modulator of Cardiac Contraction? *EMBO J.* **1995**, *14* (9), 1952−1960.

(4) Mamidi, R.; Gresham, K. S.; Li, J.; Stelzer, J. E. Cardiac Myosin Binding Protein-C Ser 302 Phosphorylation Regulates Cardiac β-Adrenergic Reserve. *Sci. Adv.* **2017**, *3* (3), e1602445.

(5) Moss, R. L.; Fitzsimons, D. P.; Ralphe, J. C. Cardiac MyBP-C Regulates the Rate and Force of Contraction in Mammalian Myocardium. *Circ. Res.* **2015**, *116* (1), 183−192.

(6) Mamidi, R.; Gresham, K. S.; Verma, S.; Stelzer, J. E. Cardiac Myosin Binding Protein-C Phosphorylation Modulates Myofilament Length-Dependent Activation. *Front. Physiol.* **2016**, *7* (2), 38.

(7) Carrier, L.; Mearini, G.; Stathopoulou, K.; Cuello, F. Cardiac Myosin-Binding Protein C (MYBPC3) in Cardiac Pathophysiology. *Gene* **2015**, *573* (2), 188−197.

(8) Main, A.; Fuller, W.; Baillie, G. S. Post-Translational Regulation of Cardiac Myosin Binding Protein-C: A Graphical Review. *Cell. Signal.* **2020**, *76*, 109788.

(9) Tong, C. W.; Stelzer, J. E.; Greaser, M. L.; Powers, P. A.; Moss, R. L. Acceleration of Crossbridge Kinetics by Protein Kinase A Phosphorylation of Cardiac Myosin Binding Protein C Modulates Cardiac Function. *Circ. Res.* **2008**, *103* (9), 974−982.

(10) Belknap, B.; Harris, S. P.; White, H. D. Modulation of Thin Filament Activation of Myosin ATP Hydrolysis by N-Terminal Domains of Cardiac Myosin Binding Protein-C. *Biochemistry* **2014**, *53* (42), 6717−6724.

(11) Colson, B. A.; Bekyarova, T.; Locher, M. R.; Fitzsimons, D. P.; Irving, T. C.; Moss, R. L. Protein Kinase A-Mediated Phosphorylation of Cmybp-c Increases Proximity of Myosin Heads to Actin in Resting Myocardium. *Circ. Res.* **2008**, *103* (3), 244−251.

(12) Coulton, A. T.; Stelzer, J. E. Cardiac Myosin Binding Protein C and Its Phosphorylation Regulate Multiple Steps in the Cross-Bridge Cycle of Muscle Contraction. *Biochemistry* **2012**, *51* (15), 3292−3301.
(13) Li, J.; Mamidi, R.; Doh, C. Y.; Holmes, J. B.; Bharambe, N.; Ramachandran, R.; Stelzer, J. E. AAV9 Gene Transfer of CMyBPC N-Terminal Domains Ameliorates Cardiomyopathy in CMyBPC-Deficient Mice. *JCI insight* **2020**, *5* (17), 0−18.
(14) Mun, J. Y.; Previs, M. J.; Yu, H. Y.; Gulick, J.; Tobacman, L. S.; Previs, S. B.; Robbins, J.; Warshaw, D. M.; Craig, R. Myosin-Binding Protein C Displaces Tropomyosin to Activate Cardiac Thin Filaments and Governs Their Speed by an Independent Mechanism. *Proc. Natl. Acad. Sci. U. S. A.* **2014**, *111* (6), 2170−2175.
(15) Gresham, K. S.; Stelzer, J. E. The Contributions of Cardiac Myosin Binding Protein C and Troponin I Phosphorylation to β-Adrenergic Enhancement of in Vivo Cardiac Function. *J. Physiol.* **2016**, *594* (3), 669−686.
(16) Gresham, K. S.; Mamidi, R.; Stelzer, J. E. The Contribution of Cardiac Myosin Binding Protein-c Ser282 Phosphorylation to the Rate of Force Generation and in Vivo Cardiac Contractility. *J. Physiol.* **2014**, *592* (17), 3747−3765.
(17) Barefield, D.; Sadayappan, S. Phosphorylation and Function of Cardiac Myosin Binding Protein-C in Health and Disease. *J. Mol. Cell. Cardiol.* **2010**, *48* (5), 866−875.
(18) Gupta, M. K.; Robbins, J. Post-Translational Control of Cardiac Hemodynamics through Myosin Binding Protein C. *Pflugers Arch.* **2014**, *466* (2), 231−236.
(19) Jia, W.; Shaffer, J. F.; Harris, S. P.; Leary, J. A. Identification of Novel Protein Kinase A Phosphorylation Sites in the M-Domain of Human and Murine Cardiac Myosin Binding Protein-C Using Mass Spectrometry Analysis. *J. Proteome Res.* **2010**, *9* (4), 1843−1853.
(20) Yuan, C.; Guo, Y.; Ravi, R.; Przyklenk, K.; Shilkofski, N.; Diez, R.; Cole, R. N.; Murphy, A. M. Myosin Binding Protein C Is Differentially Phosphorylated upon Myocardial Stunning in Canine and Rat Hearts– Evidence for Novel Phosphorylation Sites. *Proteomics* **2006**, *6* (14), 4176−4186.
(21) Rosas, P. C.; Warren, C. M.; Creed, H. A.; Trzeciakowski, J. P.; Solaro, R. J.; Tong, C. W. Cardiac Myosin Binding Protein-C Phosphorylation Mitigates Age-Related Cardiac Dysfunction. *JACC Basic to Transl. Sci.* **2019**, *4* (7), 817−830.
(22) El-Armouche, A.; Pohlmann, L.; Schlossarek, S.; Starbatty, J.; Yeh, Y. H.; Nattel, S.; Dobrev, D.; Eschenhagen, T.; Carrier, L. Decreased Phosphorylation Levels of Cardiac Myosin-Binding Protein-C in Human and Experimental Heart Failure. *J. Mol. Cell. Cardiol.* **2007**, *43* (2), 223−229.
(23) Jacques, A. M.; Copeland, O.; Messer, A. E.; Gallon, C. E.; King, K.; McKenna, W. J.; Tsang, V. T.; Marston, S. B. Myosin Binding Protein C Phosphorylation in Normal, Hypertrophic and Failing Human Heart Muscle. *J. Mol. Cell. Cardiol.* **2008**, *45* (2), 209−216.
(24) Copeland, O.; Sadayappan, S.; Messer, A. E.; Steinen, G. J. M.; van der Velden, J.; Marston, S. B. Analysis of Cardiac Myosin Binding Protein-C Phosphorylation in Human Heart Muscle. *J. Mol. Cell. Cardiol.* **2010**, *49* (6), 1003−1011.
(25) Kooij, V.; Holewinski, R. J.; Murphy, A. M.; Van Eyk, J. E. Characterization of the Cardiac Myosin Binding Protein-C Phosphoproteome in Healthy and Failing Human Hearts. *J. Mol. Cell. Cardiol.* **2013**, *60* (1), 116−120.
(26) Budde, H.; Hassoun, R.; Tangos, M.; Zhazykbayeva, S.; Herwig, M.; Varatnitskaya, M.; Sieme, M.; Delalat, S.; Sultana, I.; Kolijn, D.; Gömöri, K.; Jarkas, M.; Lódi, M.; Jaquet, K.; Kovács, Á.; Mannherz, H. G.; Sequeira, V.; Mügge, A.; Leichert, L. I.; Sossalla, S.; Hamdani, N. The Interplay between S-Glutathionylation and Phosphorylation of Cardiac Troponin I and Myosin Binding Protein C in End-Stage Human Failing Hearts. *Antioxidants* **2021**, *10* (7), 1134.
(27) El-Armouche, A.; Boknik, P.; Eschenhagen, T.; Carrier, L.; Knaut, M.; Ravens, U.; Dobrev, D. Molecular Determinants of Altered Ca 2+ Handling in Human Chronic Atrial Fibrillation. *Circulation* **2006**, *114* (7), 670−680.
(28) Decker, R. S.; Decker, M. L.; Kulikovskaya, I.; Nakamura, S.; Lee, D. C.; Harris, K.; Klocke, F. J.; Winegrad, S. Myosin-Binding Protein C Phosphorylation, Myofibril Structure, and Contractile Function during Low-Flow Ischemia. *Circulation* **2005**, *111* (7), 906−912.
(29) Previs, M. J.; Mun, J. Y.; Michalek, A. J.; Previs, S. B.; Gulick, J.; Robbins, J.; Warshaw, D. M.; Craig, R. Phosphorylation and Calcium Antagonistically Tune Myosin-Binding Protein C's Structure and Function. *Proc. Natl. Acad. Sci. U. S. A.* **2016**, *113* (12), 3239−3244.
(30) Oakley, C. E.; Hambly, B. D.; Curmi, P. M. G.; Brown, L. J. Myosin Binding Protein C: Structural Abnormalities in Familial Hypertrophic Cardiomyopathy. *Cell Res.* **2004**, *14* (2), 95−110.
(31) Idowu, S. M.; Gautel, M.; Perkins, S. J.; Pfuhl, M. Structure, Stability and Dynamics of the Central Domain of Cardiac Myosin Binding Protein C (MyBP-C): Implications for Multidomain Assembly and Causes for Cardiomyopathy. *J. Mol. Biol.* **2003**, *329* (4), 745−761.
(32) Ponnam, S.; Kampourakis, T. Microscale Thermophoresis Suggests a New Model of Regulation of Cardiac Myosin Function via Interaction with Cardiac Myosin Binding Protein-C. *J. Biol. Chem.* **2022**, *298*, 101485.
(33) Colson, B. A.; Thompson, A. R.; Espinoza-Fonseca, L. M.; Thomas, D. D. Site-Directed Spectroscopy of Cardiac Myosin-Binding Protein C Reveals Effects of Phosphorylation on Protein Structural Dynamics. *Proc. Natl. Acad. Sci. U. S. A.* **2016**, *113* (12), 3233−3238.
(34) Bunch, T. A.; Kanassatega, R.-S.; Lepak, V. C.; Colson, B. A. Human Cardiac Myosin−Binding Protein C Restricts Actin Structural Dynamics in a Cooperative and Phosphorylation-Sensitive Manner. *J. Biol. Chem.* **2019**, *294* (44), 16228−16240.
(35) Mohamed, A. S.; Dignam, J. D.; Schlender, K. K. Cardiac Myosin-Binding Protein C (MyBP-C): Identification of Protein Kinase A and Protein Kinase C Phosphorylation Sites. *Arch. Biochem. Biophys.* **1998**, *358* (2), 313−319.
(36) Bardswell, S. C.; Cuello, F.; Kentish, J. C.; Avkiran, M. CMyBP-C as a Promiscuous Substrate: Phosphorylation by Non-PKA Kinases and Its Potential Significance. *J. Muscle Res. Cell Motil.* **2012**, *33* (1), 53−60.
(37) Avkiran, M.; Rowland, A. J.; Cuello, F.; Haworth, R. S. Protein Kinase d in the Cardiovascular System: Emerging Roles in Health and Disease. *Circ. Res.* **2008**, *102* (2), 157−163.
(38) Dirkx, E.; Cazorla, O.; Schwenk, R. W.; Lorenzen-Schmidt, I.; Sadayappan, S.; Van Lint, J.; Carrier, L.; van Eys, G. J. J. M.; Glatz, J. F. C.; Luiken, J. J. F. P. Protein Kinase D Increases Maximal Ca 2+ -Activated Tension of Cardiomyocyte Contraction by Phosphorylation of CMyBP-C-Ser 315. *Am. J. Physiol. Circ. Physiol.* **2012**, *303* (3), H323−H331.
(39) Bardswell, S. C.; Cuello, F.; Rowland, A. J.; Sadayappan, S.; Robbins, J.; Gautel, M.; Walker, J. W.; Kentish, J. C.; Avkiran, M. Distinct Sarcomeric Substrates Are Responsible for Protein Kinase D-Mediated Regulation of Cardiac Myofilament Ca2+ Sensitivity and Cross-Bridge Cycling. *J. Biol. Chem.* **2010**, *285* (8), 5674−5682.
(40) Haworth, R. S.; Cuello, F.; Herron, T. J.; Franzen, G.; Kentish, J. C.; Gautel, M.; Avkiran, M. Protein Kinase D Is a Novel Mediator of Cardiac Troponin I Phosphorylation and Regulates Myofilament Function. *Circ. Res.* **2004**, *95* (11), 1091−1099.
(41) Lou, D. Y.; Dominguez, I.; Toselli, P.; Landesman-Bollag, E.; O'Brien, C.; Seldin, D. C. The Alpha Catalytic Subunit of Protein Kinase CK2 Is Required for Mouse Embryonic Development. *Mol. Cell. Biol.* **2008**, *28* (1), 131−139.
(42) Hauck, L.; Harms, C.; An, J.; Rohne, J.; Gertz, K.; Dietz, R.; Endres, M.; von Harsdorf, R. Protein Kinase CK2 Links Extracellular Growth Factor Signaling with the Control of P27Kip1 Stability in the Heart. *Nat. Med.* **2008**, *14* (3), 315−324.
(43) Thoonen, R.; Giovanni, S.; Govindan, S.; Lee, D. I.; Wang, G.-R.; Calamaras, T. D.; Takimoto, E.; Kass, D. A.; Sadayappan, S.; Blanton, R. M. Molecular Screen Identifies Cardiac Myosin−Binding

https://doi.org/10.1021/acsomega.2c00799
ACS Omega 2022, 7, 14189−14202

Protein-C as a Protein Kinase G-Iα Substrate. *Circ. Hear. Fail.* **2015**, *8* (6), 1115−1122.
(44) Knöll, R. Myosin Binding Protein C: Implications for Signal-Transduction. *J. Muscle Res. Cell Motil.* **2012**, *33* (1), 31−42.
(45) Schumacher, J. A.; Crockett, D. K.; Elenitoba-Johnson, K. S. J.; Lim, M. S. Evaluation of Enrichment Techniques for Mass Spectrometry. *J. Mol. Diagnostics* **2007**, *9* (2), 169−177.
(46) Hornbeck, P. V.; Kornhauser, J. M.; Tkachev, S.; Zhang, B.; Skrzypek, E.; Murray, B.; Latham, V.; Sullivan, M. PhosphoSitePlus: A Comprehensive Resource for Investigating the Structure and Function of Experimentally Determined Post-Translational Modifications in Man and Mouse. *Nucleic Acids Res.* **2012**, *40* (D1), D261−D270.
(47) Lundby, A.; Andersen, M. N.; Steffensen, A. B.; Horn, H.; Kelstrup, C. D.; Francavilla, C.; Jensen, L. J.; Schmitt, N.; Thomsen, M. B.; Olsen, J. V. In Vivo Phosphoproteomics Analysis Reveals the Cardiac Targets of β-Adrenergic Receptor Signaling. *Sci. Signal.* **2013**, *6* (278), 1−14.
(48) Huttlin, E. L.; Jedrychowski, M. P.; Elias, J. E.; Goswami, T.; Rad, R.; Beausoleil, S. A.; Villén, J.; Haas, W.; Sowa, M. E.; Gygi, S. P. A Tissue-Specific Atlas of Mouse Protein Phosphorylation and Expression. *Cell* **2010**, *143* (7), 1174−1189.
(49) Eng, J. K.; McCormack, A. L.; Yates, J. R. An Approach to Correlate Tandem Mass Spectral Data of Peptides with Amino Acid Sequences in a Protein Database. *J. Am. Soc. Mass Spectrom.* **1994**, *5* (11), 976−989.
(50) Macek, B.; Gnad, F.; Soufi, B.; Kumar, C.; Olsen, J. V.; Mijakovic, I.; Mann, M. Phosphoproteome Analysis of E. Coli Reveals Evolutionary Conservation of Bacterial Ser/Thr/Tyr Phosphorylation. *Mol. Cell. Proteomics* **2008**, *7* (2), 299−307.
(51) Schastnaya, E.; Raguz Nakic, Z.; Gruber, C. H.; Doubleday, P. F.; Krishnan, A.; Johns, N. I.; Park, J.; Wang, H. H.; Sauer, U. Extensive Regulation of Enzyme Activity by Phosphorylation in Escherichia Coli. *Nat. Commun.* **2021**, *12* (1), 5650.
(52) Kirk, J. A.; Holewinski, R. J.; Crowgey, E. L.; Van Eyk, J. E. Protein Kinase G Signaling in Cardiac Pathophysiology: Impact of Proteomics on Clinical Trials. *Proteomics* **2016**, *16* (5), 894−905.
(53) Ge, Y.; Rybakova, I. N.; Xu, Q.; Moss, R. L. Top-down High-Resolution Mass Spectrometry of Cardiac Myosin Binding Protein C Revealed That Truncation Alters Protein Phosphorylation State. *Proc. Natl. Acad. Sci. U. S. A.* **2009**, *106* (31), 12658−12663.
(54) Wagner, S. A.; Beli, P.; Weinert, B. T.; Schölz, C.; Kelstrup, C. D.; Young, C.; Nielsen, M. L.; Olsen, J. V.; Brakebusch, C.; Choudhary, C. Proteomic Analyses Reveal Divergent Ubiquitylation Site Patterns in Murine Tissues. *Mol. Cell. Proteomics* **2012**, *11* (12), 1578−1585.
(55) Kensler, R. W.; Craig, R.; Moss, R. L. Phosphorylation of Cardiac Myosin Binding Protein C Releases Myosin Heads from the Surface of Cardiac Thick Filaments. *Proc. Natl. Acad. Sci. U. S. A.* **2017**, *114* (8), E1355−E1364.
(56) Michalek, A. J.; Howarth, J. W.; Gulick, J.; Previs, M. J.; Robbins, J.; Rosevear, P. R.; Warshaw, D. M. Phosphorylation Modulates the Mechanical Stability of the Cardiac Myosin-Binding Protein C Motif. *Biophys. J.* **2013**, *104* (2), 442−452.
(57) McNamara, J. W.; Singh, R. R.; Sadayappan, S. Cardiac Myosin Binding Protein-C Phosphorylation Regulates the Super-Relaxed State of Myosin. *Proc. Natl. Acad. Sci. U. S. A.* **2019**, *116* (24), 11731−11736.
(58) Nag, S.; Trivedi, D. V.; Sarkar, S. S.; Adhikari, A. S.; Sunitha, M. S.; Sutton, S.; Ruppel, K. M.; Spudich, J. A. The Myosin Mesa and the Basis of Hypercontractility Caused by Hypertrophic Cardiomyopathy Mutations. *Nat. Struct. Mol. Biol.* **2017**, *24* (6), 525−533.
(59) AL-Khayat, H. A.; Kensler, R. W.; Squire, J. M.; Marston, S. B.; Morris, E. P. Atomic Model of the Human Cardiac Muscle Myosin Filament. *Proc. Natl. Acad. Sci. U. S. A.* **2013**, *110* (1), 318−323.
(60) Zoghbi, M. E.; Woodhead, J. L.; Moss, R. L.; Craig, R. Three-Dimensional Structure of Vertebrate Cardiac Muscle Myosin Filaments. *Proc. Natl. Acad. Sci. U. S. A.* **2008**, *105* (7), 2386−2390.
(61) Rahmanseresht, S.; Lee, K. H.; O'Leary, T. S.; McNamara, J. W.; Sadayappan, S.; Robbins, J.; Warshaw, D. M.; Craig, R.; Previs, M. J. The N Terminus of Myosin-Binding Protein C Extends toward Actin Filaments in Intact Cardiac Muscle. *J. Gen. Physiol.* **2021**, *153* (3), e202012726.
(62) Luther, P. K.; Winkler, H.; Taylor, K.; Zoghbi, M. E.; Craig, R.; Padrón, R.; Squire, J. M.; Liu, J. Direct Visualization of Myosin-Binding Protein C Bridging Myosin and Actin Filaments in Intact Muscle. *Proc. Natl. Acad. Sci. U. S. A.* **2011**, *108* (28), 11423−11428.
(63) Previs, M. J.; Previs, S. B.; Gulick, J.; Robbins, J.; Warshaw, D. M. Molecular Mechanics of Cardiac Myosin-Binding Protein C in Native Thick Filaments. *Science (80-.).* **2012**, *337* (6099), 1215−1218.
(64) Nelson, S. R.; Li, A.; Beck-Previs, S.; Kennedy, G. G.; Warshaw, D. M. Imaging ATP Consumption in Resting Skeletal Muscle: One Molecule at a Time. *Biophys. J.* **2020**, *119* (6), 1050−1055.
(65) Patel, B. G.; Wilder, T.; Solaro, R. J. Novel Control of Cardiac Myofilament Response to Calcium by S-Glutathionylation at Specific Sites of Myosin Binding Protein C. *Front. Physiol.* **2013**, *4*, 2−11.
(66) Stathopoulou, K.; Wittig, I.; Heidler, J.; Piasecki, A.; Richter, F.; Diering, S.; Velden, J.; Buck, F.; Donzelli, S.; Schröder, E.; Wijnker, P. J. M.; Voigt, N.; Dobrev, D.; Sadayappan, S.; Eschenhagen, T.; Carrier, L.; Eaton, P.; Cuello, F. S -glutathiolation Impairs Phosphoregulation and Function of Cardiac Myosin-binding Protein C in Human Heart Failure. *FASEB J.* **2016**, *30* (5), 1849−1864.
(67) Fert-Bober, J.; Sokolove, J. Proteomics of Citrullination in Cardiovascular Disease. *PROTEOMICS - Clin. Appl.* **2014**, *8* (7−8), 522−533.
(68) Sarikas, A.; Carrier, L.; Schenke, C.; Doll, D.; Flavigny, J.; Lindenberg, K.; Eschenhagen, T.; Zolk, O. Impairment of the Ubiquitin?Proteasome System by Truncated Cardiac Myosin Binding Protein C Mutants. *Cardiovasc. Res.* **2005**, *66* (1), 33−44.
(69) Ponnam, S.; Sevrieva, I.; Sun, Y.-B.; Irving, M.; Kampourakis, T. Site-Specific Phosphorylation of Myosin Binding Protein-C Coordinates Thin and Thick Filament Activation in Cardiac Muscle. *Proc. Natl. Acad. Sci. U. S. A.* **2019**, *116* (31), 15485−15494.
(70) Kuster, D. W. D.; Sequeira, V.; Najafi, A.; Boontje, N. M.; Wijnker, P. J. M.; Witjas-Paalberends, E. R.; Marston, S. B.; dos Remedios, C. G.; Carrier, L.; Demmers, J. A. A.; Redwood, C.; Sadayappan, S.; van der Velden, J. GSK3β Phosphorylates Newly Identified Site in the Proline-Alanine−Rich Region of Cardiac Myosin−Binding Protein C and Alters Cross-Bridge Cycling Kinetics in Human. *Circ. Res.* **2013**, *112* (4), 633−639.
(71) Chait, B. T. Mass Spectrometry: Bottom-Up or Top-Down? *Science (80-.)* **2006**, *314* (5796), 65−66.
(72) Harris, S. P.; Bartley, C. R.; Hacker, T. A.; McDonald, K. S.; Douglas, P. S.; Greaser, M. L.; Powers, P. A.; Moss, R. L. Hypertrophic Cardiomyopathy in Cardiac Myosin Binding Protein-C Knockout Mice. *Circ. Res.* **2002**, *90* (5), 594−601.
(73) Prasad, K.-M. R.; Xu, Y.; Yang, Z.; Acton, S. T.; French, B. A. Robust Cardiomyocyte-Specific Gene Expression Following Systemic Injection of AAV: In Vivo Gene Delivery Follows a Poisson Distribution. *Gene Ther.* **2011**, *18* (1), 43−52.
(74) Lock, M.; Alvira, M.; Vandenberghe, L. H.; Samanta, A.; Toelen, J.; Debyser, Z.; Wilson, J. M. Rapid, Simple, and Versatile Manufacturing of Recombinant Adeno-Associated Viral Vectors at Scale. *Hum. Gene Ther.* **2010**, *21* (10), 1259−1271.
(75) Bunch, T. A.; Lepak, V. C.; Kanassatega, R.-S.; Colson, B. A. N-Terminal Extension in Cardiac Myosin-Binding Protein C Regulates Myofilament Binding. *J. Mol. Cell. Cardiol.* **2018**, *125*, 140−148.
(76) Doh, C. Y.; Li, J.; Mamidi, R.; Stelzer, J. E. The HCM-Causing Y235S CMyBPC Mutation Accelerates Contractile Function by Altering C1 Domain Structure. *Biochim. Biophys. Acta - Mol. Basis Dis.* **2019**, *1865* (3), 661−677.
(77) Madeira, F.; Park, Y. M.; Lee, J.; Buso, N.; Gur, T.; Madhusoodanan, N.; Basutkar, P.; Tivey, A. R. N.; Potter, S. C.; Finn, R. D.; Lopez, R. The EMBL-EBI Search and Sequence Analysis Tools APIs in 2019. *Nucleic Acids Res.* **2019**, *47* (W1), W636−W641.
(78) Gasteiger, E.; Hoogland, C.; Gattiker, A.; Duvaud, S.; Wilkins, M. R.; Appel, R. D.; Bairoch, A. Protein Identification and Analysis Tools on the ExPASy Server. In *The Proteomics Protocols Handbook*;

https://doi.org/10.1021/acsomega.2c00799
ACS Omega 2022, 7, 14189−14202

Walker, J. M., Ed.; Humana Press: Totowa, NJ, 2005; pp 571−607. DOI: 10.1385/1-59259-890-0:571.
(79) Micsonai, A.; Wien, F.; Bulyáki, É.; Kun, J.; Moussong, É.; Lee, Y. H.; Goto, Y.; Réfrégiers, M.; Kardos, J. BeStSel: A Web Server for Accurate Protein Secondary Structure Prediction and Fold Recognition from the Circular Dichroism Spectra. *Nucleic Acids Res.* **2018**, *46* (W1), W315−W322.
(80) Whitmore, L.; Wallace, B. A. DICHROWEB, an Online Server for Protein Secondary Structure Analyses from Circular Dichroism Spectroscopic Data. *Nucleic Acids Res.* **2004**, *32*, W668−W673.
(81) Candiano, G.; Bruschi, M.; Musante, L.; Santucci, L.; Ghiggeri, G. M.; Carnemolla, B.; Orecchia, P.; Zardi, L.; Righetti, P. G. Blue Silver: A Very Sensitive Colloidal Coomassie G-250 Staining for Proteome Analysis. *Electrophoresis* **2004**, *25* (9), 1327−1333.
(82) Schneider, C. A.; Rasband, W. S.; Eliceiri, K. W. NIH Image to ImageJ: 25 Years of Image Analysis. *Nat. Methods* **2012**, *9* (7), 671−675.
(83) Ruse, C. I.; Willard, B.; Jin, J. P.; Haas, T.; Kinter, M.; Bond, M. Quantitative Dynamics of Site-Specific Protein Phosphorylation Determined Using Liquid Chromatography Electrospray Ionization Mass Spectrometry. *Anal. Chem.* **2002**, *74* (7), 1658−1664.
(84) Willard, B. B.; Ruse, C. I.; Keightley, J. A.; Bond, M.; Kinter, M. Site-Specific Quantitation of Protein Nitration Using Liquid Chromatography/Tandem Mass Spectrometry. *Anal. Chem.* **2003**, *75* (10), 2370−2376.
(85) Berman, H. M. The Protein Data Bank. *Nucleic Acids Res.* **2000**, *28* (1), 235−242.
(86) Kelley, L. A.; Sutcliffe, M. J. OLDERADO: On-Line Database of Ensemble Representatives and Domains. *Protein Sci.* **1997**, *6* (12), 2628−2630.
(87) Yang, J.; Yan, R.; Roy, A.; Xu, D.; Poisson, J.; Zhang, Y. The I-TASSER Suite: Protein Structure and Function Prediction. *Nat. Methods* **2015**, *12* (1), 7−8.
(88) Feig, M. Local Protein Structure Refinement via Molecular Dynamics Simulations with LocPREFMD. *J. Chem. Inf. Model.* **2016**, *56* (7), 1304−1312.
(89) Heo, L.; Park, H.; Seok, C. GalaxyRefine: Protein Structure Refinement Driven by Side-Chain Repacking. *Nucleic Acids Res.* **2013**, *41*, W384−W388.
(90) Williams, C. J.; Headd, J. J.; Moriarty, N. W.; Prisant, M. G.; Videau, L. L.; Deis, L. N.; Verma, V.; Keedy, D. A.; Hintze, B. J.; Chen, V. B.; Jain, S.; Lewis, S. M.; Arendall, W. B.; Snoeyink, J.; Adams, P. D.; Lovell, S. C.; Richardson, J. S.; Richardson, D. C. MolProbity: More and Better Reference Data for Improved All-Atom Structure Validation. *Protein Sci.* **2018**, *27* (1), 293−315.
(91) Vizcaíno, J. A.; Côté, R. G.; Csordas, A.; Dianes, J. A.; Fabregat, A.; Foster, J. M.; Griss, J.; Alpi, E.; Birim, M.; Contell, J.; O'Kelly, G.; Schoenegger, A.; Ovelleiro, D.; Pérez-Riverol, Y.; Reisinger, F.; Ríos, D.; Wang, R.; Hermjakob, H. The Proteomics Identifications (PRIDE) Database and Associated Tools: Status in 2013. *Nucleic Acids Res.* **2012**, *41* (D1), D1063−D1069.
(92) Perez-Riverol, Y.; Bai, J.; Bandla, C.; García-Seisdedos, D.; Hewapathirana, S.; Kamatchinathan, S.; Kundu, D. J.; Prakash, A.; Frericks-Zipper, A.; Eisenacher, M.; Walzer, M.; Wang, S.; Brazma, A.; Vizcaíno, J. A. The PRIDE Database Resources in 2022: A Hub for Mass Spectrometry-Based Proteomics Evidences. *Nucleic Acids Res.* **2022**, *50* (D1), D543−D552.

https://doi.org/10.1021/acsomega.2c00799
ACS Omega 2022, 7, 14189−14202